Microdeformation in Heterogeneous Polymers, Revealed by Electron Microscopy

*Christopher J.G. Plummer,**[1] *Philippe Béguelin,*[2] *Chrystelle Grein,*[2] *Rudolph Gensler,*[2] *Laure Dupuits,*[1] *Cedric Gaillard,*[3] *Pierre Stadelmann,*[3] *Hans-Henning Kausch,*[2] *Jan-Anders E. Månson*[1]

[1]Laboratoire de Technologie de Composites et Polymères (LTC), IMX-STI, Ecole Polytechnique Fédérale de Lausanne (EPFL), CH-1015, Switzerland

E-mail: christopher.plummer@epfl.ch

[2]Laboratoire de Polymères (LP), IMX-STI, Ecole Polytechnique Fédérale de Lausanne (EPFL), CH-1015, Switzerland

[3]Centre Interdisciplinaire de Microscopie Electronique (CIME), SB, Ecole Polytechnique Fédérale de Lausanne (EPFL), CH-1015, Switzerland

Summary: Recent investigations of the tensile fracture behaviour of representative glassy and semicrystalline impact-resistant polymers are reviewed, with emphasis on the microdeformation behaviour as revealed by electron microscopy of sections from bulk specimens, where the crack-tip damage zone has been embedded and/or stained under load, and on thin films deformed *in situ*. The insight that such techniques have provided into the toughening mechanisms is discussed.

Keywords: deformation; electron microscopy; fracture; high speed testing; polymers

Introduction

Polymers that require a high degree of fracture resistance are often combined with a second phase toughener. A classic example is high impact polystyrene (HIPS), a generic term for polystyrene (PS) that contains rubbery inclusions, whose role is to promote dissipative deformation and hence increase crack initiation and propagation resistance. Conventional impact tests provide a useful measure of fracture resistance at overall deformation rates equivalent to between roughly 1 and 4 m/s. Such tests are limited in scope, however, and there is growing interest in quasi-static tensile testing, which gives access to intrinsic fracture toughness parameters over a wide range of test

© 2004 International Union of Pure and Applied Chemistry DOI: 10.1002/masy.200451008

speeds, including impact speeds, and hence facilitates the systematic investigation of rate effects [1]. A parameter commonly used is the critical stress intensity factor for crack initiation in plane strain mode I opening, K_{IC} (generally the most severe test of a polymer's fracture resistance). However, a working description of the impact response may also require an indication of whether crack propagation is stable or unstable, i.e. whether failure is ductile or brittle. Indeed, in many applications, the aim is not so much to prevent failure as to ensure that it occurs via stable crack propagation, as in the case of materials for airbag housing, where it is important to minimize damage to the airbag and/or the user from flying debris during deployment.

Although fracture mechanics can provide an objective description of crack resistance, it is also important to identify the underlying microdeformation mechanisms, particularly in heterogeneous impact polymers, where crack tip deformation is often strongly dependent on the modifier properties, content and geometry. In conventional polymer matrices, there are two main types of irreversible deformation: cavitational deformation in the form of crazes, and "shear deformation", which usually refers to isovolumetric, i.e. non-cavitational plastic, deformation. Crazing is a localized deformation mode, favoured by the hydrostatic stress concentrations around crack tips in thick specimens under load, whereas shear deformation must be cooperative throughout the specimen thickness in order for the constant volume criterion to be satisfied. The connectivity of the craze fibrils means that their failure strength may be reached at craze widths of only a few μm, so that if only one craze is present at the crack tip, say, little energy is dissipated during crack advance and failure is macroscopically brittle [2, 3]. In materials such as PS, in which crazing is the dominant microdeformation mechanism, the stated aim of toughening strategies is therefore often to promote multiple craze nucleation [4-6]. Cavitation or debonding of either rubber or mineral particles, and indeed crazing itself, may nevertheless relax triaxial constraints on the matrix material at the crack tip sufficiently to favour shear yielding, which may in turn provide an important contribution to energy dissipation [4-8]. Recent work has also suggested that in semicrystalline polymers such as polyamide 6 (PA6) and polyethylene (PE), modifier particles may orient the lamellae locally so as to reduce the effective yield stress [9-13].

In what follows, after a brief description of the experimental approach, the crack-tip deformation behaviour of two types of toughened polymer will be discussed and compared. The first is rubber-

toughened glassy amorphous polymethylmethacrylate (PMMA), toughened with of a variety of tailored preformed composite particles. The second is semicrystalline isotactic polypropylene (iPP), whose T_g is below ambient temperature, but which also shows craze-like deformation and brittle impact behaviour, particularly at low molar masses. In addition to rubber toughening of iPP, which usually involves blending with an un-crosslinked modifier, efforts to improve intrinsic toughness by modification of its crystalline structure will be discussed.

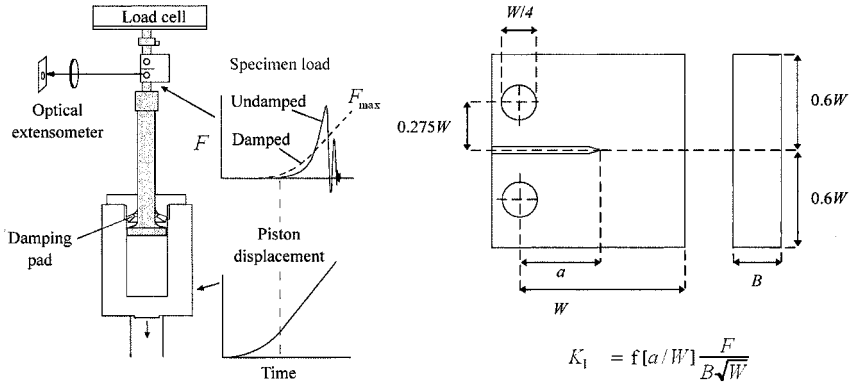

Figure 1. Set-up for high-speed testing with the CT geometry (left hand side), and the method for calculating K_I from the data (a is the crack length, F is the force, B is the specimen thickness, W is the specimen width and f[a/W] is a geometrical factor related to the specimen geometry).

Experimental

Mechanical testing: Mode I fracture tests have been carried out on compact tension (CT) specimens using a Schenck Hydropuls POZ 1152 servo-hydraulic test apparatus (Figure 1). At test speeds, $v > 0.1$ ms^{-1}, a damping pad attenuates dynamic effects, and so maintains quasi-static conditions up to the highest v (about 10 ms^{-1}) [1, 14, 15]. A mode I stress intensity factor, K_I, may then be calculated as indicated in Figure 1. If the specimen response is linear elastic up to the maximum force, F_{max}, substitution of F_{max} for F in the expression for K_I gives K_{IC}. The ductile-brittle transition is defined as the transition from stable or partly stable crack propagation (that is, $F > 0$ at displacements beyond that corresponding to F_{max}), to unstable crack propagation. In the

regimes of relatively ductile behaviour that accompany stable crack propagation, K_{IC} may be difficult to determine rigorously for practically attainable specimen thicknesses, owing to curvature of the force displacement curves [16]. The nominal critical stress intensity derived from the force maximum nevertheless provides a conservative measure of the crack initiation resistance, and remains useful for comparing different materials and the influence of materials characteristics and test parameters. Therefore, for the present purposes, no distinction is made between "valid" and "invalid" K_{IC} data.

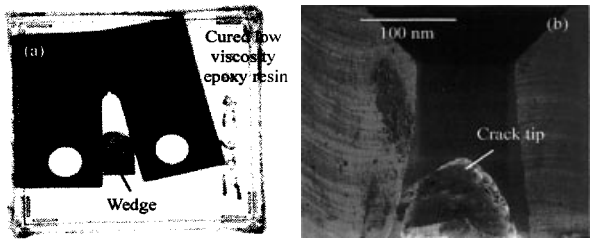

Figure 2. Specimen preparation: (a) deformed specimen with a wedge in place, mounted in epoxy resin; (b) region around the crack tip trimmed for sectioning and SEM or TEM observation [17].

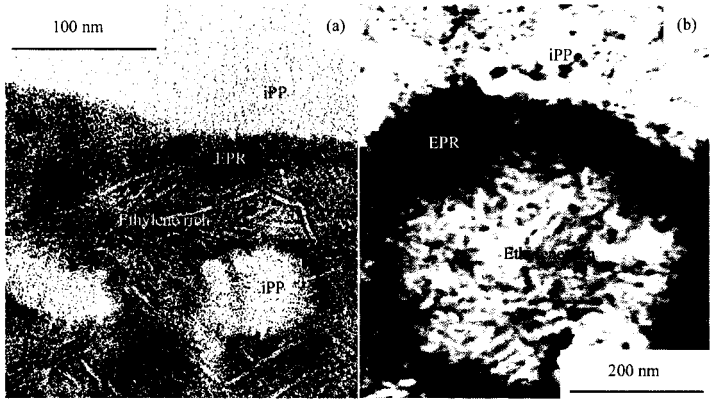

Figure 3. Modifier morphology in iPP blended with EPR: (a) TEM (Philips EM430, 300 kV, bright field, RuO_4 stained) (b) LV-SEM (Philips XL30 SFEG, 3 kV, TLD, RuO_4 stained, contrast inverted to facilitate comparison with the TEM image).

Morphological characterisation: Because crazes and other types of cavitational deformation undergo relaxation and collapse on unloading, they may need to be embedded in a low viscosity epoxy or acetate resin under load and/or marked using a suitable stain prior to sectioning for transmission electron microscopy (TEM) [14, 17, 18]. This is conveniently achieved in notched specimens by inserting a wedge between the crack faces (Figure 2). Similar techniques may also be used for low-voltage, high-resolution scanning electron microscopy (LV-SEM) [19-21]. Indeed, LV-SEM [22] and atomic force microscopy (AFM) and related near-field techniques [23] are now challenging the dominance of TEM at the length scales of the order of 10 nm that characterise not only microdeformation (voids, fibrils) but also structural components of semicrystalline and impact toughened polymers (crystallite thicknesses, modifier particles). If a backscattered electron (BSE) detector or "through-the-lens" detector (TLD) is employed in conjunction with LV-SEM, for example, staining provides sufficient chemical contrast to permit identification of individual lamellae, as illustrated in Figure 3, which compares TEM and LV-SEM images of the modifier morphology in a rubber toughened iPP.

Thin film techniques: TEM of thin, electron transparent films, deformed *in situ* by straining a copper support, which maintains them under load in the microscope, has been used extensively to investigate crazing in amorphous polymers [24]. Although easily adapted for SEM and AFM, such techniques are limited by their incompatibility with deformation on length scales comparable to or greater than the film thickness, e.g. coarse cavitation in semicrystalline polymers [25, 26], and difficulties in obtaining microstructures representative of bulk polymers with *ad hoc* preparation methods such as solvent casting. It is therefore often of interest to prepare thin sections directly from bulk polymers by ultramicrotomy [8, 27, 28]. To deform thin films at impact speeds, use has been made here of a simple apparatus based on the same principle as for the high-speed testing of bulk specimens, i.e. quasi-instant acceleration of the specimen fixture to the required speed using a pre-accelerated falling weight [8].

Rubber-toughened PMMA

PMMA is an amorphous thermoplastic with good optical characteristics, but in which crack propagation during tensile failure of notched specimens is typically characterised by a single crack

tip craze and hence relatively brittle behaviour. This is particularly true at high deformation rates, reflecting a trend towards crazing at high v and low T, whereas shear deformation dominates as T approaches T_g [29]. The challenge is to improve impact resistance in PMMA without sacrificing optical properties, so that it may replace polymers that are tougher, but more expensive, or inorganic glasses in applications such as car windows, where safety requires substantial energy absorption during impact. Emulsion polymerization offers considerable design freedom for modifier particle morphology and size, which can be fixed by crosslinking during synthesis, and hence maintained on dispersion in a PMMA matrix or matrix precursor [30-32]. Homogeneous dispersion and particle-matrix adhesion are assured by the presence of a graft PMMA outer shell. In commercial grades, the composition of the layers is adjusted to ensure transparency [30].

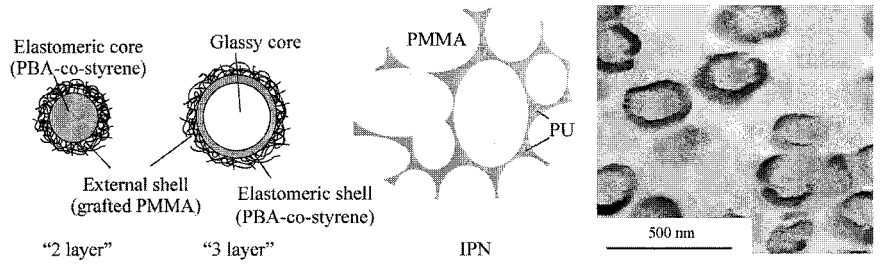

Figure 4. Modifier morphologies in rubber-toughened PMMA, along with a LV-SEM micrograph of a specimen that contains 47 wt.-% 3 layer particles (3 kV, TLD, RuO_4 stained, contrast inverted).

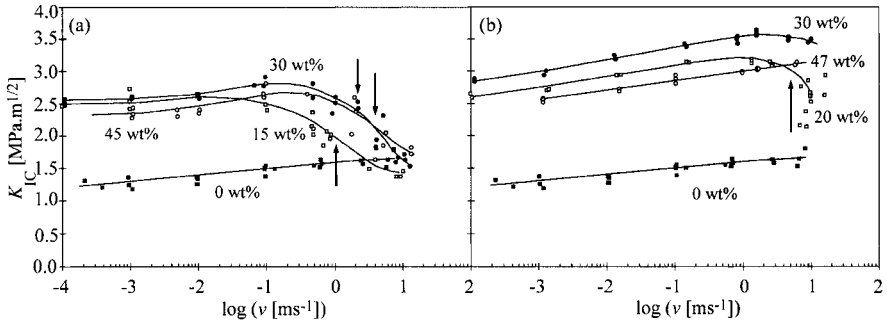

Figure 5. K_{IC} as a function of v in (a) 2 layer (b) 3 layer particle toughened PMMA for different particle contents: the PMMA matrix (0 wt% modifier) is brittle throughout whereas fully ductile behaviour is observed with 30 and 47 wt% 3 layer particles, and the remaining materials show a ductile-brittle transition indicated by the arrows [14]. (Matrix M_w = 130 kg/mol, optimized particle diameters (160 and 250 nm for the 2 and 3 layer particles respectively).

Typical modifier morphologies are shown schematically in Figure 4, along with a micrograph from a bulk specimen of toughened PMMA. Modifier particles in which the rubbery phase is restricted to a shell ("3 layer particles") give better stiffness than an equivalent loading of particles with rubbery cores ("2 layer particles"). Moreover, as illustrated in Figure 5a and b, which give room temperature results for K_{IC} as a function of v, 3 layer particles may also lead to significant improvements in K_{IC}, and a displacement of the ductile-brittle transition to higher v at fixed modifier content [33-35]. Thus, although 2 layer particles give little or no improvement over the neat matrix at the highest v, 3 layer particle contents of 30 wt% or more result in stable crack propagation over the whole range investigated [8, 14].

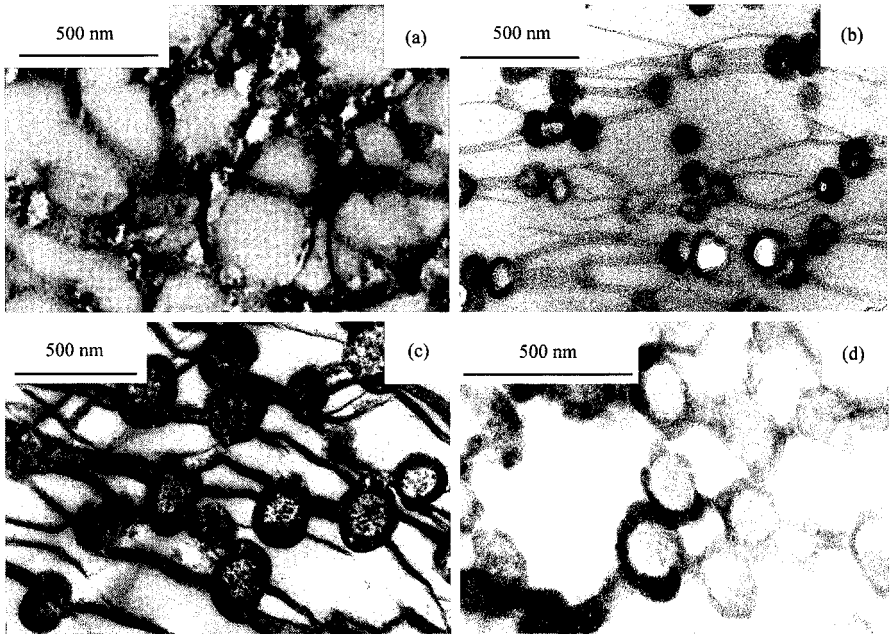

Figure 6. TEM of crack-tip deformation in CT specimens of different types of toughened PMMA deformed at about 1 mm/s at room temperature: (a) cavitation in the rubbery phase of an IPN; (b) cavitation and crazing in a specimen containing 15 wt% 2 layer particles; (c) cavitation and crazing in a specimen containing 30 wt% 3 layer particles; (d) cavitation and crazing in a specimen containing 15 wt% 3 layer particles (all specimens stained in RuO_4 prior to sectioning, tensile axis roughly vertical in each case) [8, 14].

Microdeformation in bulk specimens: Direct observations of crack tip deformation are shown in Figure 6 for different toughened PMMAs deformed at 1 mm/s, i.e. well within the regime of stable crack propagation. Also shown is crack-tip deformation in a crosslinked PMMA-based interpenetrating network (IPN) in which the modifier phase (polyurethane, PU) forms a continuous network, shown schematically in Figure 4 [36]. In the particle toughened PMMAs, stable crack propagation is accompanied by intense stress whitening, due to the formation of a network of cavitated particles and crazes. Crazing does not occur in the IPN, however, presumably owing to crosslinking, which hinders cavitation in the matrix [2]. The observation of comparable values of K_{IC} in the IPN and PMMA/30 wt% 3 layer particles and fully stable crack

propagation [8] therefore points to the primordial role of shear deformation in energy dissipation at the crack tip. Cavitation of the IPN rubbery phase (about 6 wt% of the material), visible in Figure 6a, is expected to lead to similar constraint release and crack shielding to those resulting from the formation of a continuous network of cavities and crazes in the particle toughened PMMA [8, 14, 35]. For the PMMAs with relatively low particle contents, on the other hand, crazing and constraint release are less efficient, leading to more brittle behaviour. Moreover, whereas cavitation of the rubbery shells of 3 layer particles results in load-bearing craze-like fibrillar structures uniformly distributed among the particles (as reflected by distortion and/or fibrillation of the particle cores at high deformations), cavitation of the 2 layer particles is relatively non-uniform. The corresponding large voids in the cores of certain of the 2 layer particles (Figure 6b) have been suggested to constitute weak spots in the deformed material [28].

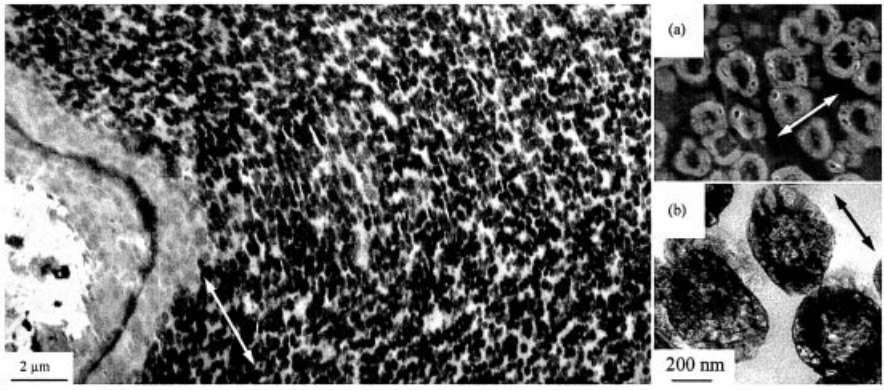

Figure 7. Crack tip deformation in a chemically modified PMMA reinforced with 47 wt% 3 layer particles and deformed at 0.1 mm/s; the insets show details of particle deformation by (a) LV-SEM and (b) TEM (all specimens stained with RuO_4, tensile axis indicated by the arrows) [37].

At particle contents approaching 50 wt%, cavitation remains prevalent in the shells of the 3 layer particles, but crazing is limited, and extensive shear deformation may be inferred from the distortion of the modifier particles near the crack tip. Indeed, in this case, constraint release and the increased matrix ligament stresses are sufficient to reduce the overall effective yield stress, and hence the nominal K_{IC}, as the particle content increases from 30 wt% to 47 wt% (Figure 5).

Similar qualitative behaviour is seen in a more ductile chemically modified PMMA matrix with twice the entanglement density of PMMA and T_g ≈85 °C, as compared with 100 °C for PMMA. Here, crazing is fully suppressed in favour of shear deformation at low v (Figure 7). Indeed, in spite of the lower T_g, K_{IC} is slightly greater than that of the conventional PMMA matrix at the same loading [37], suggesting crazing to have a negative effect in this limit.

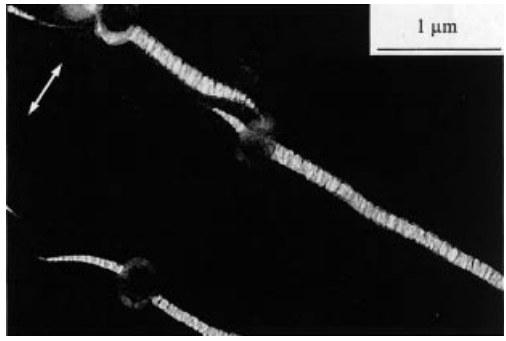

Figure 8. TEM of a thin film containing 15 wt% 3 layer particles deformed at about 1 m/s [29].

Thin film microdeformation: Among the disadvantages of direct observation of microdeformation in bulk specimens is the need to stain to obtain adequate contrast, which obscures details of the morphology. Given the relatively small length scales involved in the microdeformation of PMMA toughened with 3 layer particles, *in situ* deformation of thin films is therefore a useful complement to bulk studies. Voided regions (either modifier particles or crazes) may easily be seen by TEM without staining, provided low dose conditions are used to avoid beam damage. It is also straightforward to carry out systematic observations over a wide range of conditions using thin films, since no additional specimen preparation is required. Figures 8 and 9 give examples of deformation in films of about 300 nm in thickness prepared by microtoming bulk specimens. Figure 8a shows a thin film containing 15 wt% 3 layer particles deformed at 1 m/s showing isolated crazes with relatively straight trajectories, corresponding to the onset of brittle behaviour in the bulk fracture specimens (the undeformed particles are not visible in the micrograph). Figure 9 shows thin films taken from specimens of PMMA and the modified ductile PMMA with 47 wt% 3 layer particles and deformed at different speeds. The

fibrillar structure of the cavitated particle shells is visible in each case, and crazing is fully suppressed in the more ductile matrix at 0.1 mm/s (cf. Figure 7). At high v the tendency to craze increases, with numerous "short sharp" crazes emanating from the modifier particles in both materials, although deformation remains highly delocalized, consistent with the ductile impact response of the corresponding bulk specimens.

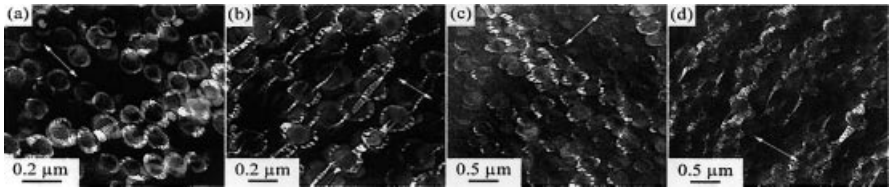

Figure 9. Thin films of PMMA containing 47 wt% 3 layer particles deformed at (a) 0.1 mm/s and (b) 1 m/s and chemically modified PMMA (cf. Figure 7) containing 47 wt% 3 layer particles deformed at (c) 0.1 mm/s and (c) 1 m/s [37] (tensile direction indicated by the arrows).

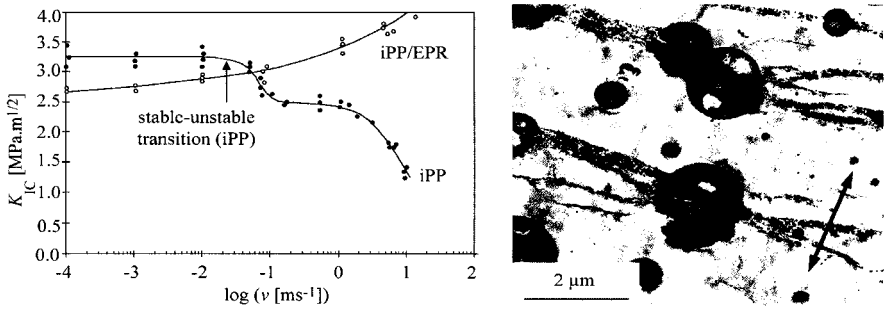

Figure 10. K_{IC} as a function of v in iPP with M_w = 455 kg/mol and iPP with M_w = 435 kg/mol containing 15 wt% EPR; the image shows modifier particle cavitation and crazing in iPP/EPR deformed at about 1 m/s and stained with RuO_4 [38].

Isotactic polypropylene

Unlike commercial grades of PMMA, iPP is often relatively crack resistant at low v. However, its impact properties remain a limiting factor in applications, owing to ductile-brittle transitions such as that shown in Figure 10 [38]. These reflect an increased tendency to craze at high v and low T for fixed M, as in PMMA. The ductile-brittle transitions are also relatively sensitive to M in the

range corresponding to commercial materials. Thus, ductile-brittle transitions at fixed T and v are also induced when M is reduced (e.g. by thermal degradation [39]). A craze microstructure typical of bulk iPP is shown in Figure 11a, with fibril diameters comparable with those in crazes in glassy polymers (around 10 nm [40]). Extensive interlamellar cavitation may also occur in the early stages of deformation as a precursor to craze formation. This is conveniently observed using thin films (Figure 11b), although the lack of plastic constraint in these latter favours diffuse lamellar shear (Figure 11c), rather than the development of well-defined craze morphology, as deformation proceeds. Given that typical modifier particle diameters (see below) are also generally much greater than the thin film thicknesses required for TEM, thin film techniques are therefore of somewhat limited relevance to bulk deformation in this case.

In bulk fracture specimens, ductile behaviour is generally characterised by stress whitening and the formation of a wedge-shaped deformation zone of multiple crazing and/or shear deformation at the crack tip. However, at impact speeds, a single narrow craze is observed, propagating normal to the principal stress axis, as shown in Figure 12, which implies crazing in this regime to be insensitive to the local morphology [17].

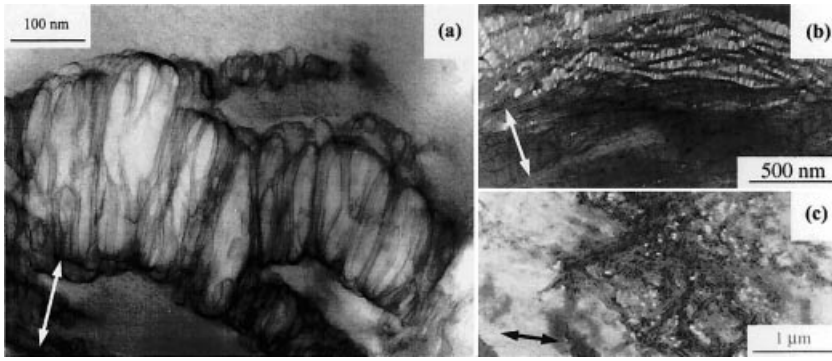

Figure 11. (a) Fibrillar deformation in bulk α iPP deformed at room temperature, embedded in PMMA and stained with RuO_4 vapour; (b) early stages of irreversible deformation in a thin film of αiPP deformed at room temperature and post-stained with RuO_4 vapour, showing interlamellar cavitation; (c) diffuse lamellar shear in the same film [38].

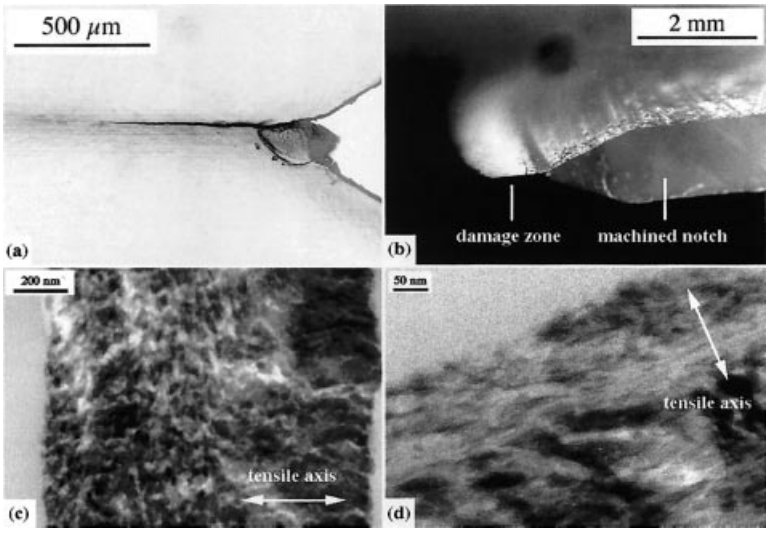

Figure 12. (a) Side-view of the crack-tip damage zone in a CT specimen of iPP with M_w of 455 kg mol^{-1} deformed at about 3 ms^{-1}; (b) oblique view of the damage zone showing the curved deformation front; (c) TEM micrograph of the collapsed fibrillar structure of the crack-tip craze; (d) detail of structure at the craze-bulk interface [18].

Influence of matrix structure: The tendency of iPP to show crazing and brittle behaviour may be linked at least partly to the unusual "cross-hatched" morphology of the relatively stable monoclinic α modification, which dominates in conventional grades under standard processing conditions [41, 42]. This morphology may block certain slip mechanisms [43, 44], and hence not only raise the yield stress but also accentuate the yield drop, thus favouring localised deformation modes such as crazing. The fracture behaviour of iPP is dependent on many other factors, large spherulites promoting brittleness, for example, owing to the concentration of structural defects and impurities at their boundaries [45]. It is nevertheless widely held, mainly on the basis of impact data, that toughness can be improved by preferential nucleation of the β phase, whose spherulites have a more conventional morphology [46-48]. Certainly, in CT tests there is a significant increase in fracture toughness in the presence of the β phase in certain ranges of T and

v, and an increase in the ductile-brittle transition speed by a least three decades at $T > T_g$ has been reported [21]. Figure 13 shows BSE-SEM images of crack-tip deformation in a β nucleated CT specimen in the ductile regime, confirming deformation to be relatively delocalized, and strongly correlated with the spherulitic structure. That crazes in α iPP are more localised and better defined than in β iPP may therefore reflect not only the influence of the cross-hatched structure on lamellar slip described in the previous section, but also the relatively homogeneous lamellar textures of α iPP spherulites. It is nevertheless difficult to exclude other factors, such as crystallinity and spherulite size, as well as the intrinsically higher molecular mobility of β iPP, purely on the basis of such microscopic observations [21].

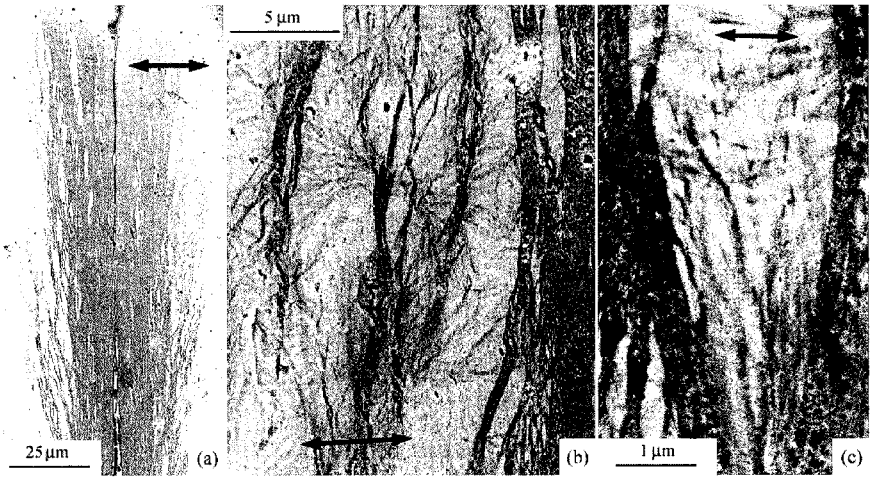

Figure 13. BSE-SEM images of crack-tip microdeformation in iPP containing approximately 80 wt% β phase tested at 0.001 ms^{-1} and 25 °C and stained with RuO_4: (i) overview of the crack tip damage zone; (ii) and (iii) details from the periphery of the damage zone. The arrows indicate the loading direction [21].

Rubber toughened iPP: Rubber toughened grades of iPP are available with a wide range of formulations and microstructures. The most common modifiers are ethylene propylene rubber (EPR), often introduced by varying the composition during synthesis (reactor blending) and ethylene-propylene-diene monomer elastomer (EPDM) [49]. A corresponding diversity of factors

contribute to mechanical performance (modifier T_g and content, particle size and size distribution, modifier morphology, interfacial strength, matrix plasticization, crystallinity and phase behaviour, and matrix molecular architecture [50-56]). Although the particles are introduced by blending rather than as prefabricated entities with precise morphologies, loss in stiffness at high modifier contents can again be moderated by using modifiers that adopt core-shell morphologies, such as shown in Figure 3, where the particle cores consist of ethylene-rich semicrystalline inclusions.

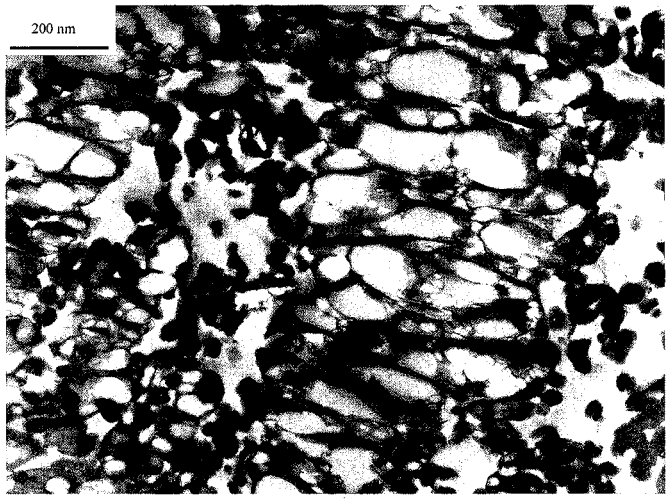

Figure 14. TEM of deformation close to the crack tip in a bulk specimen of iPP containing 52 vol% EPDM (RuO_4 stained, tensile axis roughly horizontal) [58].

As in PMMA, a primary function of rubber toughening is to delocalize crack-tip deformation; the stiffness mismatch between the matrix and modifier leads to local stress concentrations at the particle equators, promoting nucleation of crazes or precursor regions of interlamellar cavitation, as shown in Figure 10, for example. The accompanying plastic constraint release may then favour ductile drawing of the interparticle ligaments. Moreover, at high discrete particle contents, achievable in iPP toughened with EPDM vulcanates, for example, constraint release due to particle cavitation is sufficient for crazing to be entirely replaced by ductile drawing of the interparticle ligaments over a wide range of conditions, as described previously for PMMA. In the example shown in Figure 14, cavitation occurred along rows of particles aligned roughly

perpendicular to the tensile axis, sometimes referred to as "croids" [57], the subsequent necking of the intervening matrix ligaments leading to structures analogous to crazes, albeit at very different length scales [58].

Matrix properties and their dependence on test conditions are also important for the performance of toughened iPP [59, 60]. The effect of M closely follows that of untoughened iPP, with low M favouring crazing and brittle behaviour, and high M favouring shear deformation. Crazing is also favoured over homogeneous deformation in the toughened materials at high speeds and low temperatures, although this does not necessarily lead to brittle behaviour [61]. Indeed, toughening, as reflected by improvements in K_{IC}, say, is most marked in regimes of v in which the untoughened matrix is brittle, i.e. in regimes in which crazing dominates. In the example shown in Figure 10, the toughness continues to increase with increasing v beyond the ductile-brittle transition of the untoughened matrix, although at the highest v the behaviour becomes difficult to interpret, owing to significant adiabatic heating at the crack-tip. (A 90 K rise in temperature has been reported for toughened iPP at speeds of 10 ms^{-1} [54].) Moreover, β nucleation has little effect on the brittle-ductile transition of rubber-toughened iPP at any temperature. Given the important role of the rubber particles in initiating matrix deformation during crack initiation and propagation, this supports the earlier suggestion that improvements in toughness of the homopolymer on β nucleation are mainly morphological in origin [21].

Conclusions

Different morphologies and/or modifier contents can lead to surprisingly similar fracture behaviour in bulk PMMA, although the microdeformation behaviour, as revealed by TEM and LV-SEM, varies considerably. Widespread crazing of the matrix associated with cavitation of the rubbery phase is generally associated with ductile behaviour in PMMA with intermediate spherical modifier particle contents. However, results for IPNs and high spherical particle contents indicate that crazing is not always essential for toughening. The fundamental requirement is suggested to be the establishment of a continuous network of cavities and low shear modulus material (rubber or crazed material), able to release triaxial constraints on shear deformation. There are strong parallels between the microdeformation behaviour of toughened

iPP and PMMA in this respect, crazing becomes limited in both materials as the modifier content approaches 50 wt.-%. Moreover, there is a trend to more brittle behaviour with increasing test speed in both cases, which may be accounted for in terms of the time-dependence of damage development. Transitions to unstable crack propagation, i.e. macroscopically brittle behaviour, may be seen as a response of the material over timescales in which delocalized deformation in the matrix is kinetically limited, as reflected by the observation of a single crack-tip craze in bulk specimens, or isolated crazes in thin films of toughened PMMA. Indeed, in certain toughened PMMAs, thin film studies are particularly useful for identifying such trends in the microdeformation behaviour, and are therefore of direct relevance to bulk fracture, whilst at the same time giving access to a wealth of local detail that the staining techniques necessary for bulk specimens may obscure.

Acknowledgments

We acknowledge the generous financial support of TotalFinaElf, Ciba Speciality Chemicals and the Swiss CTI during the course of this work, and the technical support of the Electron Microscopy Centre (CIME) of the EPFL.

[1] P. Béguelin, H.-H. Kausch, in *"Impact and Dynamic Fracture of Polymers and Composites"*, J. G. Williams, A. Pavan, Eds., Mechanical Engineering Publications, London 1995.
[2] E. J. Kramer, *Adv. Polym. Sci.* **1983**, *52-53*, 1.
[3] H. R. Brown, *Macromolecules* **1991**, *24*, 2752.
[4] C. B. Bucknall, *"Toughened Plastics"*, Appl. Sci. Publishers, London 1977.
[5] C. K. Riew, A. J. Kinloch, Eds., *"Toughening of Plastics II"*, ACS Symposium Series 252, ACS, Washington DC 1996.
[6] R. A. Pearson, H.-J. Sue, A. F. Yee, Eds., *"Toughening of Plastics: Advances in Modelling and Experiments"*, ACS Symposium Series 759, ACS, Washington DC 2000.
[7] A. M. L. Magalhães, R. J. M. Borggreve, *Macromolecules* **1995**, *28*, 5841.
[8] C. J. G. Plummer, P. Béguelin, H.-H. Kausch, *Colloids and Surfaces A* **1999**, *153*, 551.
[9] Z. Bartczack, A. S. Argon, R. E. Cohen, M. Weinberg, *Polymer* **1999**, *40*, 2331.
[10] Z. Bartczack, A. S. Argon, R. E. Cohen, M. Weinberg, *Polymer* **1999**, *40*, 2347.
[11] R. J. M. Borggreve, R. J. Gaymans, J. Schuijer, J. F. Ingen Housz, *Polymer* **1989**, *28*, 1489.
[12] S. Wu, *Polymer* **1985**, *26*, 1855.
[13] S. Wu, *J. Appl. Poly. Sci.* **1988**, *35*, 549.
[14] P. Béguelin, PhD Thesis, EPFL, 1996.
[15] P. Béguelin, C. Fond, H.-H. Kausch, *Int. J. Fracture* **1998**, *89*, 85.
[16] J.G. Williams, "*Fracture Mechanics of Polymers*", Ellis Horwood, Chichister UK 1984.
[17] C.J.G. Plummer, P. Scaramuzzino, H.-H. Kausch, *Polym. Eng. & Sci.* **2000**, *40*, 1306.

[18] R. Gensler, C. J. G. Plummer, C. Grein, H.-H. Kausch, *Polymer* **2000**, *41*, 3809.
[19] K. Friedrich, *Adv. Polym. Sci.* **1983**, *52-53*, 225.
[20] H.B.H. Hamouda, M. Simaos-Betbeder, F. Grillon, P. Blouet , N. Billon, R. Piques, *Polymer* **2001**, *42*, 5425.
[21] C. Grein, C. J. G. Plummer, H.-H. Kausch, Y. Germain, P. Béguelin, *Polymer* **2002**, *43*, 3279.
[22] J. H. Butler, D. C. Joy, G. F. Bradley, S. J. Krause, *Polymer* **1995**, *36*, 1781.
[23] G. Binning, C. F. Quate, C. Gerber, *Phys. Rev. Lett.* **1986**, *56*, 930.
[24] B. D. Lauterwasser, E. J. Kramer, *Phil. Mag.* **1979**, *39A*, 469.
[25] C. J. G. Plummer, H.-H. Kausch, *Macromol. Chem. Phys.* **1996**, *197*, 2047.
[26] C. J. G. Plummer, H.-H. Kausch, *J. Macromol. Sci. - Phys.* **1996**, *B35*, 637.
[27] G. H. Michler, *Trends in Polymer Science* **1995**, *3*, 124.
[28] C. J. G. Plummer, P. Béguelin, H.-H. Kausch, *Polymer* **1996**, *37*, 7.
[29] C. J. G. Plummer, L. Tézé, J. L. Halary, L. Monnerie, H.-H. Kausch, *Polymer* **1996**, *37*, 19.
[30] P. A. Lovell, *Trends in Polymer Science* **1996**, *4*, 264.
[31] P. A. Lovell, J. McDonald, D. E. J. Saunders, M. N. Sherratt, R. J. Young, in *"Toughened Plastics I"*, C. K. Riew, A. J. Kinloch, Eds., ACS, Washington DC 1993.
[32] P. A. Lovell, M. M. Sherratt, R. J. Young, in *"Toughened Plastics II"*, C. K. Riew, A. J. Kinloch, Eds., ACS, Washington DC 1996.
[33] C. J. Hooley, D. R. Moore, M. Whale, M. J. Williams, *Plast. Rubber Processing & Applications* **1981**, *1*, 345.
[34] O. Julien, P. Béguelin, L. Monnerie, H.-H. Kausch, in "*Toughened Plastics II*", C.K. Riew, A.J. Kinloch, Eds. ACS, Washington DC 1996.
[35] P. Béguelin, C. J. G. Plummer, H.-H. Kausch, in "*Polymer Blends and Alloys*", G. O. Shonaike, G. P. Simon, Eds., Marcel Dekker, New York 1999.
[36] P. Heim, C. Wrotecki, M. Avenel, P. Gaillard, *Polymer* **1993**, *34*, 1653.
[37] L. Dupuits, C. J. G. Plummer, P. Gerard, J.-A. E. Månson, *Proc. Int. Conf. on Deformation, Yield and Fracture of Polymers*, Cambridge, 7-10 April 2003, p. 399.
[38] R. Gensler, PhD Thesis, EPFL, 1998.
[39] R. Gensler, C. J. G. Plummer, H.-H. Kausch, E. Kramer, J.-R. Pauquet, H. Zweifel, *Polym. Degrad. & Stab.* **2001**, *67*, 195.
[40] C. J. G. Plummer, C. Creton, F. Kalb, L. Léger, *Macromolecules* **1998**, *31*, 6164.
[41] R. H. Olley, D. C. Bassett, *Polymer* **1989**, *30*, 399.
[42] D. R. Norton, A. Keller, *Polymer* **1985**, *26*, 704.
[43] M. Aboulfaraj, C. G'Sell, B. Ulrich, A. Dahoun, *Polymer* **1995**, *36*, 731.
[44] G. Coulon, G. Castelein, C. G'Sell, *Polymer* **1999**, *40*, 95.
[45] K. Friedrich, U. A. Karsch, *J. Mater. Sci.* **1981**, *16*, 2167.
[46] J. Karger-Kocsis, J. Varga, G. W. Ehrenstein, *J. Appl. Polym. Sci.* **1997**, *64*, 2057.
[47] S. C. Tjong, J. S. Shen, R. K. Y. Li, *Scripta Metallurgica et Materialia* **1995**, *33*, 503.
[48] M. W. Gahleitner, *J. Appl. Polym. Sci.* **1996**, *61*, 649.
[49] J. Karger-Kocsis, Ed. "*Polypropylene - an A to Z reference*", Kluwer, Dodrecht 1999.
[50] D. Dompas, G. Groeninckx, M. Isogawa, T. Hasegawa, M. Kadokura, *Polymer Commun.* **1995**, *36*, 437.
[51] A. van der Wal, R. Nijhof, R. J. Gaymans, *Polymer* **1999**, *40*, 6031.
[52] A. van der Wal, A. J. J. Verheul, R. J. Gaymans, *Polymer* **1999**, *40*, 6067.
[53] A. van der Wal, A. J. J. Verheul, R. J. Gaymans, *Polymer* **1999**, *40*, 6057.
[54] A. van der Wal, R. J. Gaymans, *Polymer* **1999**, *40*, 6045.
[55] B. Dukanszky, F. Tudos, A. Kallo, G. Bodor, *Polymer* **1989**, *30*, 1399.
[56] F. Ramsteiner, *Acta Polymerica* **1991**, *42*, 584.
[57] H.-J. Sue, *J. Mater. Sci.* **1992**, *27*, 3098.
[58] F. Kalb, L. Léger, C. J. G. Plummer, C. Creton, P. Marcus, A. M. L. Magalhaes, *Macromolecules* **2001**, *34*, 2702.
[59] A. van der Wal, J. J. Mulder, R. J. Gaymans, *Polymer* **1998**, *39*, 5467.
[60] A. van der Wal, J. J. Mulder, R. J. Gaymans, *Polymer* **1998**, *39*, 5477.
[61] B. Z. Jang, D. R. Uhlmann, J. B. Van der Sande, *J. Appl. Polym. Sci.* **1985** *30*, 2485.